

Article

A Finite-Time Sliding Mode Control Approach for Constrained Euler–Lagrange System

Guhao Sun  and Qingshuang Zeng *

School of Astronautics, Harbin Institute of Technology, Harbin 150001, China; sungh@hit.edu.cn

* Correspondence: zqshuang@hit.edu.cn

Abstract: This paper investigates a general control strategy to track the reference trajectory for the constrained Euler–Lagrange system with model uncertainties and unknown external disturbances. Unlike the disturbances assumed to be upper-bounded by a constant in other papers, we consider the disturbances to be bounded by a function of the system states, which are more realistic. First, the nominal controller was designed based on the nonsingular fast terminal sliding mode control, and global fast finite-time convergence to the sliding surface was guaranteed. As the system is state-constrained in this paper, we introduce the control barrier function approach to formulate the constraints and ensure the system does not break the restrictions. The proposed control strategy was numerically assessed on a two-link robot manipulator system, and the simulation results illustrate the effectiveness of the proposed control strategy.

Keywords: Euler–Lagrange system; terminal sliding mode control; control barrier function; nonsingularity; finite-time convergence

MSC: 93D40



Citation: Sun, G.; Zeng, Q. A Finite-Time Sliding Mode Control Approach for Constrained Euler–Lagrange System. *Mathematics* **2023**, *11*, 2788. <https://doi.org/10.3390/math11122788>

Academic Editors: Fang Liu and Qianyi Liu

Received: 12 May 2023
Revised: 15 June 2023
Accepted: 19 June 2023
Published: 20 June 2023



Copyright: © 2023 by the authors. Licensee MDPI, Basel, Switzerland. This article is an open access article distributed under the terms and conditions of the Creative Commons Attribution (CC BY) license (<https://creativecommons.org/licenses/by/4.0/>).

1. Introduction

The Euler–Lagrange system, as a mechanical system that is widely used in robotics, such as unmanned ground vehicles [1,2], unmanned air vehicles [3,4], robot manipulators [5,6], satellites [7], and so on, has been of broad interest in recent years. The system model is derived from the kinetic equations and the Euler–Lagrange equation. Consequently, it is worthy of further research, especially in practical applications. Moreover, as a typical motion control system, controller design based on the Euler–Lagrange system model is more versatile and dumbs down the designing process. Nonetheless, the sophistication of the dynamics makes it challenging to identify the system parameters for a specific robot. Given the vital importance of the linear in parameters (LIP) property [8] of the Euler–Lagrange system, estimating the uncertainties is achievable via an appropriate observer [1,7]. In addition, the Euler–Lagrange system is highly nonlinear and constantly affected by various external unknown disturbances. Hence, for the trajectory tracking control of the Euler–Lagrange system, researchers have introduced various advanced control strategies to solve the above issues in the actual control scenario, such as model predictive control [9,10] and sliding mode control [11].

As more attention has been paid to swarm behavior in insects and birds, approaches involving individual behavior have certain limitations, especially in complex task scenarios. Through the cooperation between multiple agents, work efficiency and reliability can be improved. Even if a single or part of the agents fails, the system can remain functional through appropriate reactions. Most agents can be modeled as a Euler–Lagrange system, even for a heterogeneous multiagent system. Recently, researchers have increasingly focused on multiagent cooperative control based on the Euler–Lagrange system [12,13].

Unlike classical control theory, which is drawn from engineering practice and focuses on the system’s dynamic performance, the modern control approach is based on stability

analysis theory, i.e., designing the controller to guarantee the system converges to the equilibrium point. In practice, the rapid convergence of the system has a very significant impact on the control performance, especially in environments that require high dynamics.

Sliding mode control (SMC) is one of the most effective control approaches as a result of its insensitivity to certain external disturbances and model uncertainties. The basic idea of SMC is to steer the trajectory of the system to the sliding surface and converge to the equilibrium point. However, as a linear sliding surface is adopted, it can only guarantee the asymptotic stability of the system. Compared with the conventional sliding mode control, terminal sliding mode control (TSMC) can drive the system to the equilibrium point in finite time via a nonlinear function in the sliding surface. In [14], a continuous TSMC was tested for mechanical servo systems, which achieved robustness and finite-time convergence. Although TSMC could significantly improve the dynamic performance of the system, the singularity problem remained. A new terminal sliding surface [15] was proposed to eliminate the singularity problem. For further improvement on the convergence rate of the system, considering the different behavior of linear and nonlinear functions in different intervals, researchers proposed many improvement methods for the sliding mode surface. A robust ATNTSM control approach was introduced in [16] for robotic manipulators with finite-time convergence guaranteed based on the arctan function. It was shown that the convergence rate is apparently faster than the traditional TSMC and NTSMC. An adaptive nonsingular fast TSMC was proposed in [17] to control both the position and attitude of a quadrotor subject to model uncertainties and external disturbances.

In addition, there always exist various constraints for the agent to achieve complex tasks working in a restricted and practical environment, such as adaptive cruise control [18] and collision avoidance [19]. Model predictive control [20] is widely used for systems with constraints. However, model predictive control is a model-based optimal control approach, which means the model accuracy will affect the control performance directly. Due to the high calculation burden, more computing resources are required to solve the nonlinear optimization problem, especially in high dynamics environments. Another control approach is based on the barrier Lyapunov function. Unlike quadratic functions, the barrier will force the system to back away as it approaches the state's boundary. In [21], an adaptive fuzzy controller was proposed based on a tan-type barrier Lyapunov function to achieve trajectory tracking with output constraints. Similarly, a tan-type barrier Lyapunov-based optimized backstepping controller was proposed in [22]. While the desired signal does not break the constraints, it is hard to say whether the state constraints can be satisfied in practice. A mixed H_2/H_∞ fault-detection filtering was proposed in [23] to improve the safety and reliability of industrial processes. An observer-based fault estimation and fault-tolerant control of the linear discrete time-varying stochastic system was presented in [24].

In recent years, a safety-critical control strategy was proposed in [25] based on the set invariance theory to drive the system states into a predefined safe set. This work unifies the control Lyapunov function (CLF) with the control barrier function (CBF) through an online quadratic programming (QP) process for adaptive cruise controller design. It guarantees that the car can always go forward with the desired velocity unless the front vehicle is too close to maintain a safe distance. It has been shown that the online QP can be performed with sample rates of 200 Hz to 1 kHz in real time, which means the CLF-CBF-QP framework is an effective way to stabilize the system with additional constraints, such as state and output constraints. Similar frameworks have also been extended to various attractive applications in robotics, such as collision-free behaviors in multirobot systems [26,27], dynamic locomotion over rough terrain for quadruped robots [28], and bipedal robotic walking [29].

In this paper, we tackle the tracking problem of the constrained Euler–Lagrange system with model uncertainties and unknown external disturbances. The main contributions of this paper are summed up as follows: (i) To improve the control performance of the conventional NTSMC, we propose a novel nonsingular fast terminal sliding mode controller (NFTSMC). Compared with the algorithm in [16], the NFTSMC shows a faster convergence

rate and better robustness; (ii) the state constraints are formulated as a function-defined safe set. The tracking problem is solved using a CBF-QP, and the simulation results illustrate the effectiveness of tracking a reference signal that sometimes breaks the limits on states.

The rest of this paper is organized as follows. The Euler–Lagrange system model and some preliminaries are given in Section 2. The NFTSMC and CBF-QP control strategy is presented in Section 3, and simulation results illustrate the effectiveness of the proposed control strategy in Section 4. The paper is concluded in Section 5.

2. Dynamic Model and Preliminaries

2.1. Dynamic Model

Consider a typical Euler–Lagrange system

$$M(\ddot{q}) + C(q, \dot{q})\dot{q} + G(q) = \tau + \tau_d, \tag{1}$$

where $q, \dot{q}, \ddot{q} \in \mathbb{R}^n$ denote the generalized position, velocity, and acceleration of the system, respectively. $M(q) \in \mathbb{R}^{n \times n}$, which is symmetric positive definite denotes the inertia matrix and $C(q, \dot{q}) \in \mathbb{R}^{n \times n}$, is the centrifugal and Coriolis matrix. $G(q) \in \mathbb{R}^n$ is a generalized force caused by the potential energy. $\tau, \tau_d \in \mathbb{R}^n$ are generalized control input and external disturbances applied to the system, respectively. For the convenience, the matrices are abbreviated as M, C, G . In fact, we cannot obtain the system parameters precisely, i.e., there exists uncertain terms $\delta M, \delta C$, and δG , which can be expressed as

$$\begin{aligned} M &= M_0 + \delta M, \\ C &= C_0 + \delta C, \\ G &= G_0 + \delta G, \end{aligned}$$

where M_0, C_0 , and G_0 are estimated system parameters. Then, system (1) can be reformed as

$$M_0\ddot{q} + C_0\dot{q} + G_0 = \tau + f, \tag{2}$$

where $f = \tau_d - \delta M\ddot{q} - \delta C\dot{q} - \delta G$ is the total disturbances including model uncertainties and external disturbances.

Let $x_1 = q, x_2 = \dot{q}$, then system (2) can be rewritten as

$$\begin{cases} \dot{x}_1 = x_2, \\ \dot{x}_2 = F(x_1, x_2) + M_0^{-1}(x)\tau + d(t, x), \end{cases} \tag{3}$$

where

$$\begin{aligned} F(x_1, x_2) &= -M_0^{-1}(C_0\dot{q} + G_0), \\ d(t, x) &= M_0^{-1}f, \end{aligned}$$

The external disturbances such as friction and wind drag are bounded [15] and can be expressed as a function of the states. Then, we have the following assumption:

Assumption 1. The disturbance $d(t, x)$ is bounded by

$$\|d(t, x)\| \leq \|M_0^{-1}\|(b_0 + b_1\|q\| + b_2\|\dot{q}\|) \tag{4}$$

where b_0, b_1 , and b_2 are positive constants. Let $\rho = \|M_0^{-1}\|(b_0 + b_1\|q\| + b_2\|\dot{q}\|)$. It is trivial that $\rho > 0$.

The following lemma is given to analyze the stability of the system:

Lemma 1. *The states of the system will converge to the origin within finite time if there exists a continuous positive function $V(x) : \mathbb{R}^n \rightarrow \mathbb{R}$ for any given initial condition $x(0) = x_0$, such that [30]*

$$\dot{V}(x) \leq -\alpha_1 V(x) - \alpha_2 V^\alpha(x), \tag{5}$$

where $\alpha_1, \alpha_2 > 0, 0 < \alpha < 1$.

2.2. Conventional Nonsingular TSMC

Consider the following second-order nonlinear system with uncertainties:

$$\begin{cases} \dot{x}_1 = x_2, \\ \dot{x}_2 = f(x) + g(x)u + d(x, t), \end{cases} \tag{6}$$

where $d(x, t)$ denotes the uncertainties and external disturbances, which is bounded by $\|d(x, t)\| \leq D, g(x) \neq 0$, and D is a positive constant. Let $x = [x_1, x_2]^T$ be the state vector with $x_1 \in \mathbb{R}$ and $x_2 \in \mathbb{R}$. The nonsingular terminal sliding surface is chosen as

$$s = x_1 + \frac{1}{\beta} x_2^{\frac{p}{q}}, \tag{7}$$

where $\beta > 0$ and p, q are positive odd integers satisfying $p > q$. For system (6), the nonsingular terminal sliding mode controller is designed as

$$u = -g^{-1}(x) \left(f(x) + \beta \frac{q}{p} x_2^{2-\frac{p}{q}} + (D + \eta) \text{sign}(s) \right), \tag{8}$$

where $1 < p/q < 2, \eta > 0$. For convenience, let $\lambda = 1/\beta, \gamma = q/p$. Then, when the sliding mode motion is achieved, the states will converge to the equilibrium point within

$$T_n = \int_0^{|x_1(0)|} \frac{\lambda^{1/\gamma}}{x_1^{1/\gamma}} dx_1 = \frac{\lambda^{1/\gamma} \cdot |x_1(0)|^{1-1/\gamma}}{1-1/\gamma}. \tag{9}$$

2.3. Control Barrier Function

The basic idea of the control barrier function method is to design a barrier function that satisfies some specific conditions and keeps the safe set forward invariant.

Definition 1. *The set \mathcal{C} is the aforementioned forward invariant for system (10) if, from any initial state $x(t_0) \in \mathcal{C}$, the solutions $x(t)$ remain in that set for all $t \geq t_0$.*

Consider a general control affine system,

$$\dot{x} = f(x) + g(x)u \tag{10}$$

with f and g being locally Lipschitz, and $x \in \mathcal{X} \subseteq \mathbb{R}^n$ being the state and $u \in \mathcal{U} \subseteq \mathbb{R}^m$ the control input. A safe set \mathcal{C} is defined as

$$\mathcal{C} = \{x \in \mathbb{R}^n : h(x) \geq 0\}, \tag{11}$$

where $h(x) : \mathbb{R}^n \rightarrow \mathbb{R}$ is a continuously differentiable function and will be defined later. The safe set \mathcal{C} is forward invariant if and only if there exists a control input u , such that

$$\dot{h}(x, u) \geq -\alpha(h(x)), \tag{12}$$

where $\alpha(\cdot)$ is an extended class \mathcal{K} function that is strictly increasing and $\alpha(0) = 0$. There are many other equivalent conditions; for more details see [31] and the references therein. Then, we can have the following definition of control barrier function:

Definition 2. The function $h(x)$ is said to be a zero control barrier function if there exists an extended class \mathcal{K} function α such that [32]

$$\sup_{u \in \mathbb{R}^m} \left(L_f h(x) + L_g h(x)u + \alpha(h(x)) \right) \geq 0, \tag{13}$$

where $L_f h(x)$ and $L_g h(x)$ denote the Lie derivatives of $h(x)$ as

$$L_f h(x) = \frac{\partial h(x)}{\partial x} f(x), \quad L_g h(x) = \frac{\partial h(x)}{\partial x} g(x).$$

One of the benefits of CBF is that we can design the controller separately. Given the nominal input u_{norm} , which is intended to stabilize or tracks a reference signal for system (10), a CBF-QP problem can be expressed as

$$\begin{aligned} u^*(x) &= \arg \min_{u \in \mathbb{R}^m} \frac{1}{2} \|u - u_{\text{norm}}\|^2 \\ \text{s.t.} \quad & L_f h(x) + L_g h(x)u + \alpha(h(x)) \geq 0. \end{aligned} \tag{14}$$

The applied control input u is equivalent to the nominal one if the safe condition is satisfied. Once the system become potentially unsafe, the CBF-QP guarantees that the system will not break the safe set and that the applied control input is as close as possible to the nominal control.

3. Controller Design

In this section, an NFTSMC controller design method is given such that the Euler–Lagrange system can track a given reference trajectory within finite time with a strong antidisturbance capacity. To overcome the singularity problem in conventional TSMC design and further improve the convergence rate, inspired by [33], for the cases of relative degree higher than 1, an exponential CBF (ECBF) is used to ensure the safe set \mathcal{C} forward invariant.

3.1. NFTSM Controller Design

To achieve fast convergence and disturbance rejection, the nonsingular terminal sliding surface was designed as

$$s = x_1 + \Lambda_1 \text{sign}^{\Gamma_1}(x_1) + \Lambda_2 \text{sign}^{\Gamma_2}(x_2), \tag{15}$$

where

$$\begin{aligned} \Gamma_1 &= \text{diag}(\gamma_{11}, \gamma_{12}, \dots, \gamma_{1n}), \quad \Gamma_2 = \text{diag}(\gamma_{21}, \gamma_{22}, \dots, \gamma_{2n}) \\ \Lambda_1 &= \text{diag}(\lambda_{11}, \lambda_{12}, \dots, \lambda_{1n}), \quad \Lambda_2 = \text{diag}(\lambda_{21}, \lambda_{22}, \dots, \lambda_{2n}) \end{aligned}$$

with $\gamma_{1i} > \gamma_{2i}$, $1 < \gamma_{2i} < 2$ and $\lambda_{1i}, \lambda_{2i} > 0$ for $i = 1, 2, \dots, n$. Note that $\text{sign}^\Gamma(x)$ denotes

$$\begin{aligned} \text{sign}^\Gamma(x) &= \text{diag}(\text{sign}(x)) \cdot |x|^\Gamma \\ &= [|x_1|^{\gamma_1} \text{sign}(x_1) \ \dots \ |x_n|^{\gamma_n} \text{sign}(x_n)]^T, \end{aligned}$$

where $\text{sign}(x) = [\text{sign}(x_1) \ \dots \ \text{sign}(x_n)]^T$, $|x|^\Gamma = [|x_1|^{\gamma_1} \ \dots \ |x_n|^{\gamma_n}]^T$ and it is trivial that

$$\frac{d}{dt} \text{sign}^\Gamma(x) = \Gamma \text{diag}(|x|^{\Gamma - \mathbf{I}_n}) \cdot \dot{x},$$

where \mathbf{I}_n is an n -dimensional identity matrix. Then, we have the time derivative of (15) as

$$\dot{s} = \dot{x}_2 + \Lambda_1 \Gamma_1 \text{diag}(|x_1|^{\Gamma_1 - \mathbf{I}_n}) \dot{x}_1 + \Lambda_2 \Gamma_2 \text{diag}(|x_2|^{\Gamma_2 - \mathbf{I}_n}) \dot{x}_2. \tag{16}$$

Theorem 1. Consider the rewritten Euler–Lagrange system (3) with uncertainties and disturbances satisfying Assumption 1, the system state will converge to the origin in finite time via the following control law:

$$\begin{aligned} \tau = & -M_0 \left(M_2 s + (\rho + M_1) \frac{s}{\|s\|} - M_0^{-1} (C_0 x_2 + G_0) + \right. \\ & \left. \Lambda_2^{-1} \Gamma_2^{-1} (\mathbf{I}_n + \Lambda_1 \Gamma_1 \text{diag}(|x_1|^{\Gamma_1 - \mathbf{I}_n})) \text{sign}^{2\mathbf{I}_n - \Gamma_2}(x_2) \right), \end{aligned} \tag{17}$$

where M_1 and M_2 are positive constants.

Proof. Consider the following Lyapunov function

$$V = \frac{1}{2} s^T s. \tag{18}$$

Then, the derivative of V becomes

$$\begin{aligned} \dot{V} = & s^T \dot{s} \\ = & s^T (x_2 + \Lambda_1 \Gamma_1 \text{diag}(|x_1|^{\Gamma_1 - \mathbf{I}_n}) x_2 + \Lambda_2 \Gamma_2 \text{diag}(|x_2|^{\Gamma_2 - \mathbf{I}_n}) (F(x_1, x_2) + \\ & g(x) \tau + d(t, x))). \end{aligned} \tag{19}$$

Substituting (17) into (19), it follows that

$$\begin{aligned} \dot{V} = & s^T \left(\dot{x}_1 + \Lambda_1 \Gamma_1 \text{diag}(|x_1|^{\Gamma_1 - \mathbf{I}_n}) \dot{x}_1 + \Lambda_2 \Gamma_2 \text{diag}(|x_2|^{\Gamma_2 - \mathbf{I}_n}) \left(d - M_2 s - \right. \right. \\ & \left. \left. (\rho + M_1) \frac{s}{\|s\|} - \Lambda_2^{-1} \Gamma_2^{-1} (\mathbf{I}_n + \Lambda_1 \Gamma_1 \text{diag}(|x_1|^{\Gamma_1 - \mathbf{I}_n})) \text{sign}^{2\mathbf{I}_n - \Gamma_2}(x_2) \right) \right) \\ = & s^T \left(\dot{x}_1 + \Lambda_1 \Gamma_1 \text{diag}(|x_1|^{\Gamma_1 - \mathbf{I}_n}) \dot{x}_1 + \Lambda_2 \Gamma_2 \text{diag}(|x_2|^{\Gamma_2 - \mathbf{I}_n}) \left(d - M_2 s - \right. \right. \\ & \left. \left. (\rho + M_1) \frac{s}{\|s\|} \right) - (\mathbf{I}_n + \Lambda_1 \Gamma_1 \text{diag}(|x_1|^{\Gamma_1 - \mathbf{I}_n})) \dot{x}_1 \right) \\ = & -s^T \Lambda_2 \Gamma_2 \text{diag}(|x_2|^{\Gamma_2 - \mathbf{I}_n}) \left((\rho + M_1) \frac{s}{\|s\|} + M_2 s - d \right). \end{aligned}$$

Notice that

$$\begin{aligned} -\left(s^T \rho \frac{s}{\|s\|} - s^T d \right) & \leq -\|s\| \rho + \|s\| \cdot \|d\| \\ & \leq -\|s\| \rho + \|s\| \cdot \rho = 0. \end{aligned}$$

Therefore, it is obviously that

$$\begin{aligned} \dot{V} & \leq -s^T \Lambda_2 \Gamma_2 \text{diag}(|x_2|^{\Gamma_2 - \mathbf{I}_n}) \left(\frac{M_1}{\|s\|} + M_2 \right) s \\ & \leq -\min(\lambda_{2i} \gamma_{2i} |x_{2i}|^{\gamma_{2i} - 1}) \left(M_1 \|s\| + M_2 s^T s \right). \end{aligned}$$

Let

$$\begin{aligned} \rho_1(x_2) & = \min(\lambda_{2i} \gamma_{2i} |x_{2i}|^{\gamma_{2i} - 1}) \cdot 2M_2, \\ \rho_2(x_2) & = \min(\lambda_{2i} \gamma_{2i} |x_{2i}|^{\gamma_{2i} - 1}) \cdot \sqrt{2}M_1. \end{aligned}$$

Then, it follows that

$$\dot{V} \leq -\rho_1 V - \rho_2 \sqrt{V}, \tag{20}$$

When $x_{2i} \neq 0$, it is trivial that $\rho_1 > 0$ and $\rho_2 > 0$. By Lemma 1, it can be confirmed that the states of the system will converge to the sliding surface $s = 0$ within finite time. Then, we consider the case that $x_{2i} = 0$. Substituting (17) into (3), we have

$$\begin{aligned} \dot{x}_2 &= - (C_0 \dot{q} + G_0) - M_0 \left(M_2 s + (\rho + M_1) \frac{s}{\|s\|} - M_0^{-1} (C_0 x_2 + G_0) + \right. \\ &\quad \left. \Lambda_2^{-1} \Gamma_2^{-1} (\mathbf{I}_n + \Lambda_1 \Gamma_1 \text{diag}(|x_1|^{\Gamma_1 - \mathbf{I}_n})) \text{sign}^{2\mathbf{I}_n - \Gamma_2}(x_2) \right) + d(t, x) \\ &= - M_2 s - M_1 \frac{s}{\|s\|} + \rho \frac{s}{\|s\|} + d(t, x) \\ &\leq - M_2 s - M_1 \frac{s}{\|s\|} \end{aligned}$$

which suggests that $\dot{x}_{2i} < -M_1$ and $\dot{x}_{2i} > M_1$ for the cases $s_i > 0$ and $s_i < 0$, respectively. This indicates that the states of the system will not remain at the points $x_{2i} = 0$. It is shown in Figure 1 that the controller will drive the states to the sliding surface $s = 0$ when $x_2 = 0$. □

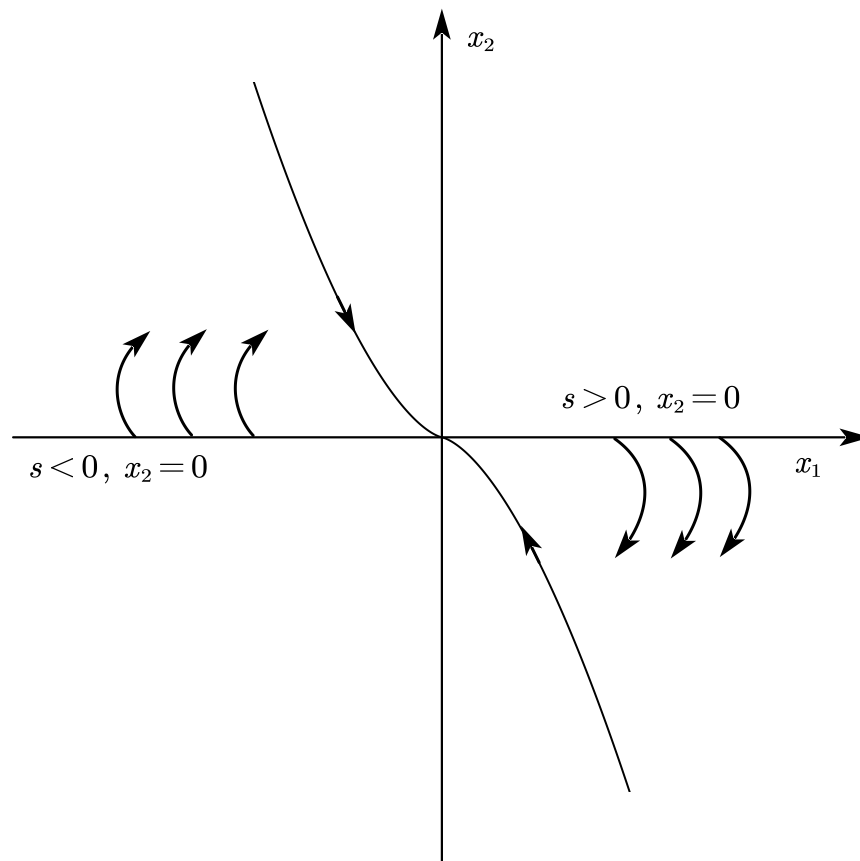


Figure 1. The phase trajectory of the system.

Remark 1. Both NFTSM and conventional TSM share a nonlinear term of tracking error to achieve fast convergence when the states are far from the origin. However, the convergence rate changes slowly when the system approaches the sliding surface. Unlike TSM, a linear term of x_1 is introduced into the sliding surface to ensure a fast rate while approaching the nearby origin. See [15,16] for more details on how the states converge to zero when the sliding surface is reached.

Proposition 1. *If the following conditions are satisfied:*

$$\lambda_i = \left(\frac{\lambda_{2i}}{\lambda_{1i}} \right)^{\frac{\gamma_i}{\gamma_{2i}}}, \gamma_i = \frac{\gamma_{2i}}{\gamma_{1i}},$$

then the states converge to the equilibrium point controlled using the NFTSMC faster than with the conventional nonsingular TSMC for any nonzero initial state $x_1(0)$. λ_i and γ_i are parameters of the conventional nonsingular TSMC given by (6).

Proof. It is trivial that

$$(x_{1i} + \lambda_{1i}x_{1i}^{\gamma_{1i}})^{\frac{1}{\gamma_{2i}}} > \lambda_{1i}^{\frac{1}{\gamma_{2i}}}x_{1i}^{\frac{\gamma_{1i}}{\gamma_{2i}}}, \tag{21}$$

which follows that

$$\begin{aligned} T_{nf} &= \int_0^{|x_{1i}(0)|} \frac{\lambda_{2i}^{\frac{1}{\gamma_{2i}}}}{(x_{1i} + \lambda_{1i}x_{1i}^{\gamma_{1i}})^{\frac{1}{\gamma_{2i}}}} dx_{1i} \\ &< \int_0^{|x_{1i}(0)|} \frac{(\lambda_{2i}/\lambda_{1i})^{1/\gamma_{2i}}}{x_{1i}^{\gamma_{1i}/\gamma_{2i}}} dx_{1i} = T_n, \end{aligned} \tag{22}$$

where T_{nf} is the convergence time of the proposed controller. Therefore, the NFTSMC converges to the equilibrium faster than the conventional nonsingular TSMC. This completes the proof. \square

Remark 2. *To reduce the chattering caused by switching, we use a continuous function in control law (17) to replace $s/\|s\|$,*

$$\Theta = \frac{s}{\|s\| + \delta'}, \tag{23}$$

where δ is a positive small constant. As δ is selected to be small enough, $\Theta \approx s/\|s\|$.

3.2. High-Order CBF Design

Without loss of generality, consider the control affine system (10). Assume that the barrier function $h(x)$ is a continuously differentiable function and satisfies

$$h^{(r)} + k_{r-1}h^{(r-1)} + \dots + k_1\dot{h} + k_0h \geq 0, \tag{24}$$

where k_0, \dots, k_{r-1} are real constants such that the roots of the following polynomial:

$$p(\lambda) = \lambda^r + k_{r-1}\lambda^{r-1} + \dots + k_1\lambda + k_0 \tag{25}$$

are all negative real, i.e., $-\lambda_1, \dots, -\lambda_r$ ($\lambda_i > 0, 1 \leq i \leq r$). We define

$$s_0(t, x) = h(x), s_k = \left(\frac{d}{dt} + \lambda_k \right) s_{k-1}, 1 \leq k \leq r. \tag{26}$$

It is obvious from (26) that (24) is equivalent to $s_r(t, x) \geq 0$. Denote $s_k(0, x(0))$ as $s_k(0)$, then we have the following lemma:

Lemma 2. *Given a continuously differentiable function $h(x)$ and a set of real constant k_0, \dots, k_{r-1} such that (24) is satisfied and the roots of polynomial (25) are all negative real [34]. If $s_i(0) \geq 0, i = 0, 1, \dots, r - 1$, then $h(x) \geq 0$ for any $t \geq 0$.*

Proof. As $s_r(t, x) \geq 0$ and (26), we have

$$\frac{d}{dt} \left(e^{\lambda_r t} s_{r-1}(t, x(t)) \right) \geq 0.$$

Integrate both sides on $[0, t]$ and we have

$$s_{r-1}(t, x(t)) \geq s_{r-1}(0)e^{-\lambda_r t}.$$

Similarly, multiply both sides by $e^{\lambda_{r-1}t}$ and from (26), we have

$$\frac{d}{dt} \left(e^{\lambda_{r-1}t} s_{r-2}(t, x(t)) \right) \geq s_{r-1}(0)e^{(\lambda_{r-1}-\lambda_r)t}.$$

After integrating, we have

$$s_{r-2}(t, x(t)) \geq s_{r-1}(0)e^{-\lambda_{r-1}t} \int_0^t e^{(\lambda_{r-1}-\lambda_r)\tau_1} d\tau_1 + s_{r-2}(0)e^{-\lambda_{r-1}t}.$$

Repeat the above iterative process and it becomes

$$s_0(t, x(t)) \geq s_0(0)e^{-\lambda_1 t} + \sum_{k=1}^{r-1} \left[s_k(0)e^{-\lambda_1 t} \int_0^t e^{(\lambda_1-\lambda_2)\tau_k} \int_0^{\tau_k} e^{(\lambda_2-\lambda_3)\tau_{k-1}} \dots \int_0^{\tau_2} e^{(\lambda_k-\lambda_{k+1})\tau_1} d\tau_1 \dots d\tau_{k-1} d\tau_k \right].$$

It is easy to check that the integral item of the above inequality is positive and, as $t \rightarrow \infty$, it converges to zero. Since $s_i(0) \geq 0$, it is trivial that $s_0(t, x(t)) \geq 0$. Therefore, $h(x) \geq 0$ for any $t \geq 0$. □

Then, we can have the following definition:

Definition 3. Given control affine system (10), the smooth function $h(x) : \mathcal{X} \rightarrow \mathbb{R}$ with relative degree r is defined as an exponential control barrier function if there exists $\mathcal{K} \in \mathbb{R}^r$, such that $\forall x \in \mathcal{C}$

$$\sup_{u \in \mathcal{U}} \left(L_f^r h(x) + L_g L_f^{r-1} h(x) u + \mathcal{K}^T \mathcal{H} \right) \geq 0,$$

where $\mathcal{K} = [k_0 \ k_1 \ \dots \ k_{r-1}]^T$ can be decided by the pole placement approach and

$$\mathcal{H} = \begin{bmatrix} h(x) \\ L_f h(x) \\ \vdots \\ L_f^{r-1} h(x) \end{bmatrix}. \tag{27}$$

For all $x \in \mathcal{X}$, define the set

$$K_{\text{ecbf}}(x) = \{u \in \mathcal{U} \mid L_f^r h(x) + L_g L_f^{r-1} h(x) u + \mathcal{K}^T \mathcal{H} \geq 0\}.$$

According to Lemma 2, we can have the following proposition:

Proposition 2. Given control affine system (10), $h(x)$ is an ECBF with relative degree r . Then, any controller $u \in K_{\text{ecbf}}$ will render the safe set \mathcal{C} defined by the (11) forward invariant.

Proposition 2 can be easily proved by Lemma 2. As defined above, the set K_{ecbf} provides a family of applicable control inputs that render the system inside the safe set. Therefore, we only need to find a proper control input inside K_{ecbf} to guarantee that the tracking performance is as accurate as possible.

We consider the state constraints as safety conditions to ensure that the Euler–Lagrange system can track the reference trajectory within state limits. Inspired by the work in [27],

we use a super-ellipsoid safety region to ensure the safety of the system. We only consider the position constraints applied to the systems, and the safe set is defined as

$$\mathcal{C} = \{ \mathbf{x} \in \mathbb{R}^{2n} : h(\mathbf{x}) \geq 0 \}, \tag{28}$$

$$h(\mathbf{x}) = 1 - \left(\frac{x_{11} - c_1}{p_1} \right)^4 - \dots - \left(\frac{x_{1n} - c_n}{p_n} \right)^4, \tag{29}$$

where x_{ij} is j th component of x_i , c_i is the center of the ellipse, and p_i is the bound on the state. By taking the derivatives of $h(\mathbf{x})$ along \mathbf{x} , we have

$$\begin{aligned} \frac{\partial h(\mathbf{x})}{\partial \mathbf{x}} &= -4 \cdot \left[\left(\frac{x_{11} - c_1}{p_1} \right)^3 \dots \left(\frac{x_{1n} - c_n}{p_n} \right)^3 \mathbf{0}_{1 \times n} \right], \\ L_f h(\mathbf{x}) &= \frac{\partial h(\mathbf{x})}{\partial \mathbf{x}} \left[\mathbf{x}_2^T \mathbf{F}(\mathbf{x}_1, \mathbf{x}_2)^T \right]^T \\ &= -4 \left(\frac{x_{11} - c_1}{p_1} \right)^3 x_{21} - 4 \left(\frac{x_{12} - c_1}{p_1} \right)^3 x_{22} - \dots - 4 \left(\frac{x_{1n} - c_1}{p_1} \right)^3 x_{2n}, \end{aligned} \tag{30}$$

$$L_g h(\mathbf{x}) = \frac{\partial h(\mathbf{x})}{\partial \mathbf{x}} \left[\mathbf{0}_{n \times n} (\mathbf{M}_0^{-1})^T \right]^T = \mathbf{0}_{1 \times n}. \tag{31}$$

Apparently, function $h(\mathbf{x})$ has relative degree two, which means the control input cannot be expressed explicitly, and the CBF-QP (14) of relative degree one is no longer applicable. Continue to take the derivative of $h(\mathbf{x})$ and we have

$$\begin{aligned} \nabla L_f h(\mathbf{x}) &= \frac{\partial L_f h(\mathbf{x})}{\partial \mathbf{x}}, \\ L_f^2 h(\mathbf{x}) &= \nabla L_f h(\mathbf{x}) \cdot \left[\mathbf{x}_2^T \mathbf{F}(\mathbf{x}_1, \mathbf{x}_2)^T \right]^T, \end{aligned} \tag{32}$$

$$L_g L_f h(\mathbf{x}) = \nabla L_f h(\mathbf{x}) \cdot \left[\mathbf{0}_{n \times n} (\mathbf{M}_0^{-1})^T \right]^T. \tag{33}$$

3.3. ECBF-Based QP Design

We can formulate the ECBF condition into a quadratic program to refine the nominal control law (17) in real time. To minimize the control deviation from the nominal one, we take the control input error as

$$\begin{aligned} \|e_u\|^2 &= (\mathbf{u} - \boldsymbol{\tau})^T (\mathbf{u} - \boldsymbol{\tau}) \\ &= \mathbf{u}^T \mathbf{u} - 2\boldsymbol{\tau}^T \mathbf{u} + \boldsymbol{\tau}^T \boldsymbol{\tau}. \end{aligned}$$

Then, we can reformulate the CBF-QP problem (14) as

$$\begin{aligned} \mathbf{u}^*(\mathbf{x}) &= \arg \min_{\mathbf{u} \in \mathbb{R}^m} \mathbf{u}^T \mathbf{u} - 2\boldsymbol{\tau}^T \mathbf{u} \\ \text{s.t. } &L_f^2 h(\mathbf{x}) + L_g L_f h(\mathbf{x}) \mathbf{u} + \mathcal{K}^T \mathcal{H} \geq 0, \end{aligned} \tag{34}$$

where $\mathcal{K} = [k_0 \ k_1]^T$, $\mathcal{H} = [h(\mathbf{x}) \ L_f h(\mathbf{x})]^T$ and $L_f h(\mathbf{x})$, $L_f^2 h(\mathbf{x})$, $L_g L_f h(\mathbf{x})$ are defined by (30)–(33), respectively.

Remark 3. Safety is always required to be satisfied even though the states of the system break the limit. When the constraints hold, the tracking error cannot converge to the origin, which means the system is unstable from this perspective. Therefore, this is a compromise between safety and performance.

4. Numerical Simulation

In this section, numerical simulations exemplify the validity and performance of the proposed control strategy. Consider a two-link robotic manipulator system [15], as shown in Figure 2, whose dynamics equation is described as an Euler–Lagrange system:

$$M(\ddot{q}) + C(q, \dot{q})\dot{q} + G(q) = \tau + \tau_d.$$

In this case, q_i denotes the angular position of the i th arm, r_i the length of the arm, m_i the mass, and J_i the moment of inertial. Denote $q = [q_1 \ q_2]^T$ as the state of the system and the relative matrices are defined as

$$M(\ddot{q}) = \begin{bmatrix} M_{11} & M_{12} \\ M_{21} & M_{22} \end{bmatrix},$$

$$C(q, \dot{q}) = \begin{bmatrix} -\beta_{12}(q_2)\dot{q}_1^2 - 2\beta_{12}(q_2)\dot{q}_1\dot{q}_2 \\ \beta_{12}(q_2)\dot{q}_2^2 \end{bmatrix},$$

$$G(q) = \begin{bmatrix} (m_1 + m_2)gr_1 \cos q_2 + m_2gr_2 \cos(q_1 + q_2) \\ m_2gr_2 \cos(q_1 + q_2) \end{bmatrix},$$

where

$$M_{11} = (m_1 + m_2)r_1^2 + m_2r_2^2 + 2m_2r_1r_2 \cos q_2 + J_1,$$

$$M_{12} = m_2r_2^2 + m_2r_1r_2 \cos q_2,$$

$$M_{21} = m_2r_2^2 + m_2r_1r_2 \cos q_2,$$

$$M_{22} = m_2r_2^2 + J_2,$$

$$\beta_{12}(q_2) = m_2r_1r_2 \sin q_2$$

with parameters given as $r_1 = 1$ m, $r_2 = 0.8$ m, $J_1 = 5$ kg m², $J_2 = 5$ kg m², $m_1 = 0.5$ kg, $m_2 = 1.5$ kg, and $g = 9.81$ m s⁻². As mentioned above, the system parameters sometimes cannot be acquired accurately and we assume that the mass is uncertain. Instead, we assume that the nominal values of m_1 and m_2 are $\hat{m}_1 = 0.4$ kg and $\hat{m}_2 = 1.2$ kg, respectively. The external disturbances are given by $\tau_d = [2 \sin(t) + 0.5 \sin(200\pi t), \cos(2t) + 0.5 \sin(200\pi t)]^T$. Select the following initial conditions: $q_{10} = 1$, $q_{20} = 0$, and the desired trajectory is given by $q_d = [-1.5 \sin(0.8t), 2.5 \cos(t)]^T$. The uncertainty term is assumed to satisfy Assumption 1 where the parameters are given by $b_0 = 12$, $b_1 = 2.2$, $b_2 = 2.8$.

Define the tracking error $\varepsilon_1 = q - q_d$ and $\varepsilon_2 = \dot{q} - \dot{q}_d$. Therefore, the tracking error model of system (3) can be expressed as

$$\begin{cases} \dot{\varepsilon}_1 = \varepsilon_2, \\ \dot{\varepsilon}_2 = F_e(\varepsilon) + M_0^{-1}(q)\tau + d(t, x), \end{cases} \tag{35}$$

where $F_e(\varepsilon) = F(x_1, x_2) - \ddot{q}_d$.

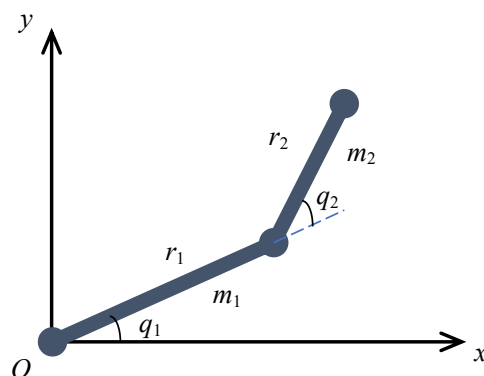


Figure 2. 2-DOF robot manipulator.

4.1. Controllers for Comparison

To demonstrate the effectiveness and robustness of the proposed NFTSM controller, we used the ANTSM control scheme proposed in [16] with the same system parameters for comparison. In addition, the ANTSM surface was chosen as

$$s = \sigma + C_a \varepsilon_2^{\alpha/\beta},$$

and the control input τ can be expressed as

$$\tau = \tau_{eq} + \tau_{sw},$$

where

$$\tau_{eq} = -M_0(q)(\Pi + F(\varepsilon)),$$

$$\tau_{sw} = -M_0(q) \left(a_0 + a_1 \|q\| + a_2 \|\dot{q}\|^2 \right) \text{sign}(\Lambda s) - k M_0(q) s,$$

and $k > 0$ is an appropriately chosen constant. The remaining parameters of the controllers are given in Table 1.

Table 1. Controller parameters.

Variables	Values	Variables	Values
M_1	1	k_0	600
M_2	2	k_1	50
Γ_1	diag([2 2])	p_1	1
Γ_2	diag([5/3 5/3])	p_2	2
Λ_1	diag([2 2])	α	5
Λ_2	diag([1 1])	β	3
C_a	diag([0.3 0.4])	k	2.5
δ_1, δ_2	3.5×10^{-3}		

The tracking performance of the given two-link robotic manipulator system is illustrated in Figures 3 and 4. As shown in Figure 3, both controllers were able to track the reference trajectory, and the NFTSM controller performed better when the system was disturbed with a relatively large amplitude signal. To further illustrate the angular position tracking performance of the controllers, the position tracking error is shown in Figure 5. The NFTSM controller ensured that the position tracking error converged to zero, while the error caused by the ANTSM controller fluctuated in a small range. As can be seen in Figure 4, the ANTSM controller also fluctuated to a certain extent during speed tracking. Although the saturation function was utilized instead of the sign function, the ANTSM control input still changed relatively sharply. Figure 6 illustrates the control signal of each joint, and it shows that no singularity indeed occurred. Figure 7 shows that the sliding surfaces converged to zero within 0.5 s, much faster than the compared ANTSMC algorithm, and finite-time convergence was achieved. A comparison of the two controllers revealed that the NFTSM controller guarantees faster convergence and has stronger robustness.

4.2. States Constrained

Considering the states were constrained, we formulated the constraints on the angular position of each joint as safe constraints, we defined the safe set by (28), and $h(x)$ was defined as

$$h(x) = 1 - \left(\frac{q_1}{p_1} \right)^4 - \left(\frac{q_2}{p_2} \right)^4. \tag{36}$$

To illustrate the effectiveness of our proposed approach, we assumed the constraints on the angular position of each joint to be $-1 \leq q_1 \leq 1$ and $-2 \leq q_2 \leq 2$, i.e., $p_1 = 1$, $p_2 = 2$. We still took $q_d = [-1.5 \sin(0.8t), 2.5 \cos(t)]^T$ as the reference trajectory, which sometimes broke the state constraints. As shown in Figure 8, when q_i was about to break

the limits, the controller responded quickly through the CBF-QP process to guarantee the states remained in the predefined safe set. When the system was operating safely, the zero tracking error with high robustness and finite-time convergence was guaranteed. The control inputs are shown in Figure 9.

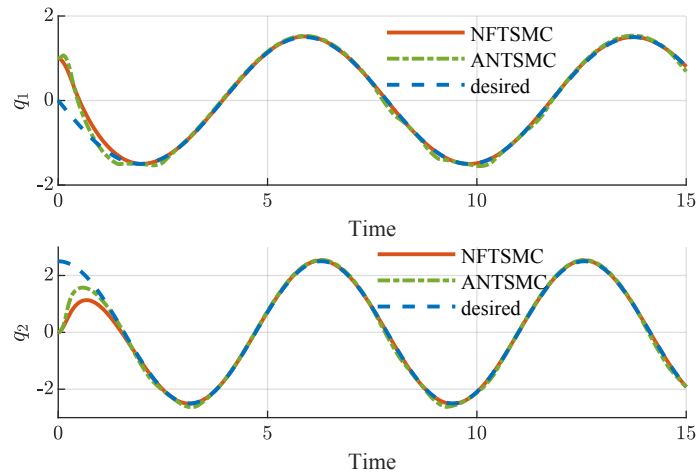


Figure 3. Angular position of joint-1 (upper) and joint-2 (lower) tracking responses to a sin-type desired trajectory with unknown external disturbances.

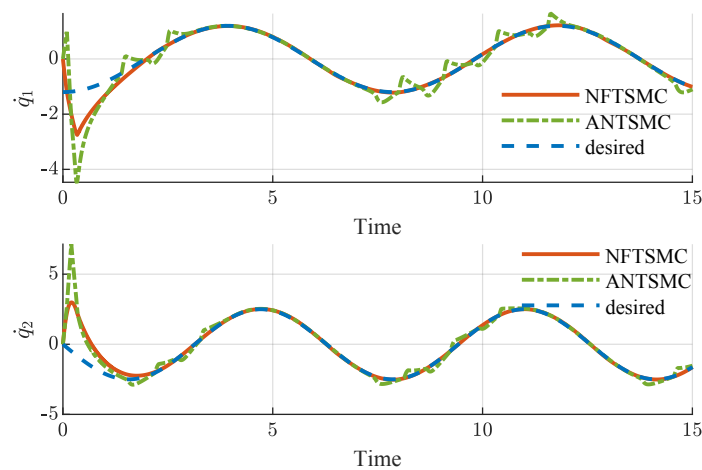


Figure 4. Angular velocity of joint-1 (upper) and joint-2 (lower) tracking responses.

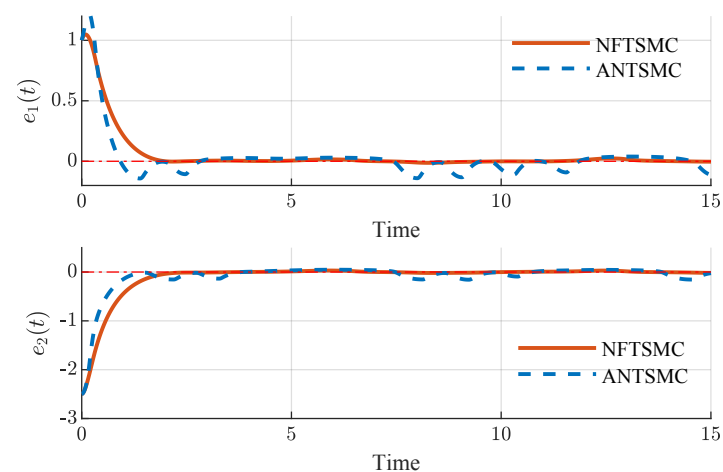


Figure 5. Angular position tracking error of joint-1 (upper) and joint-2 (lower).

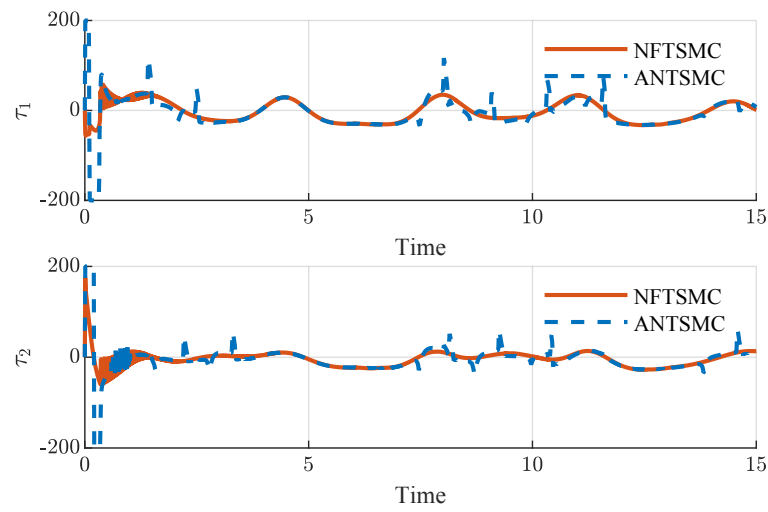


Figure 6. Control responses to the desired trajectory of joint-1 (upper) and joint-2 (lower).

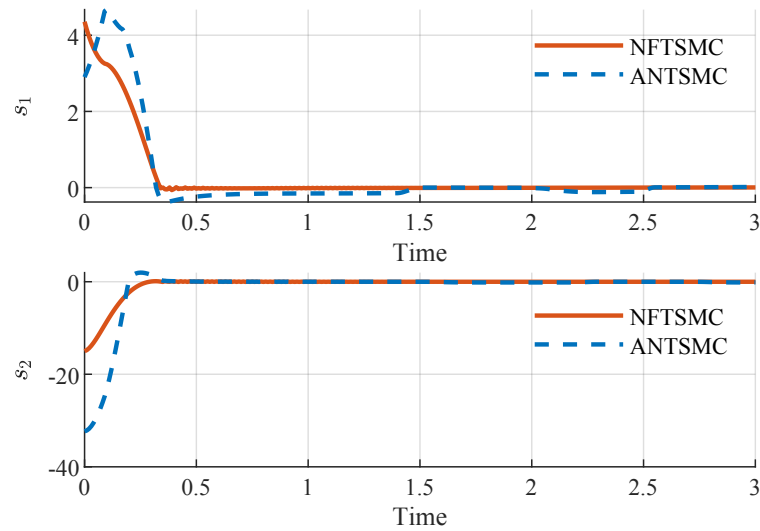


Figure 7. The time evolution of sliding surface of each joint.

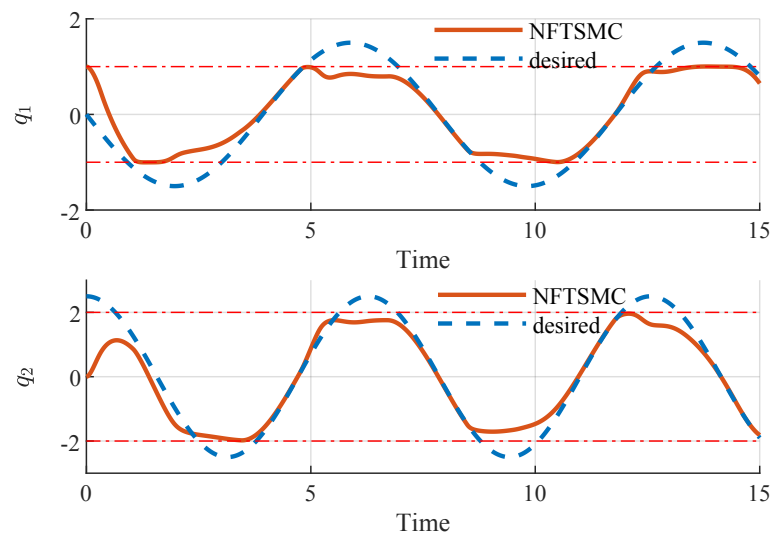


Figure 8. Trajectory tracking of the angular position with safe constraints.

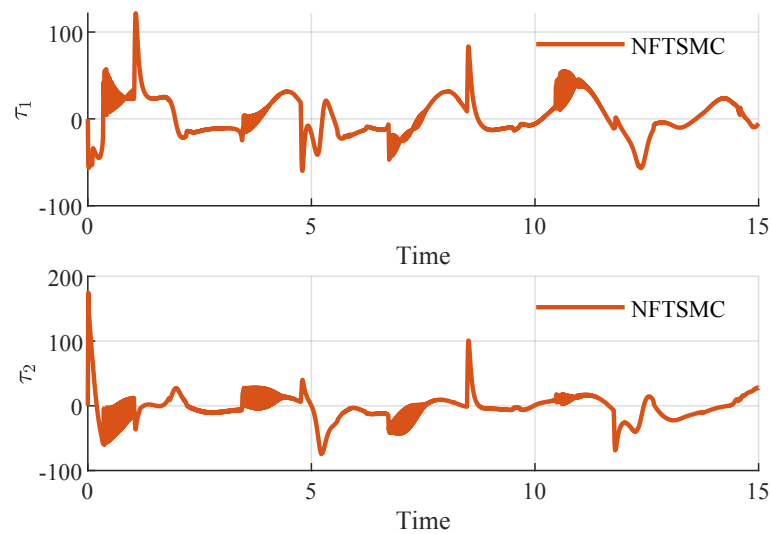


Figure 9. Trajectory tracking of the angular position with safe constraints.

4.3. Safety Behavior

We considered physical limitations on the robot manipulator system for more practical scenarios. We assumed that there was a wall above, and the joints should not hit the wall. The control purpose was to enforce the joints to the desired place without collisions. The initial position was $q_0 = [0, 0]^T$ and desired position was $q_d = [\pi, \pi]^T$. The wall was about 1.5 m high, i.e.,

$$r_1 \sin q_1 + r_2 \sin q_2 \leq 1.5.$$

Thus, we defined the control barrier function as

$$h(x) = 1.5 - r_1 \sin q_1 - r_2 \sin q_2. \tag{37}$$

We applied the CBF-QP controller to this two-link robot manipulator with the aforementioned safe constraints. Figures 10 and 11 show the trajectory of the angular position and velocity of each joint. It is shown that the robot reached the desired position in about 3 s. For a more precise illustration, the time evolution of the robot manipulator is provided in Figure 12. We can see that the joints were controlled correctly to avoid collision, while the joints controlled by the NFTSM-only controller hit the wall.

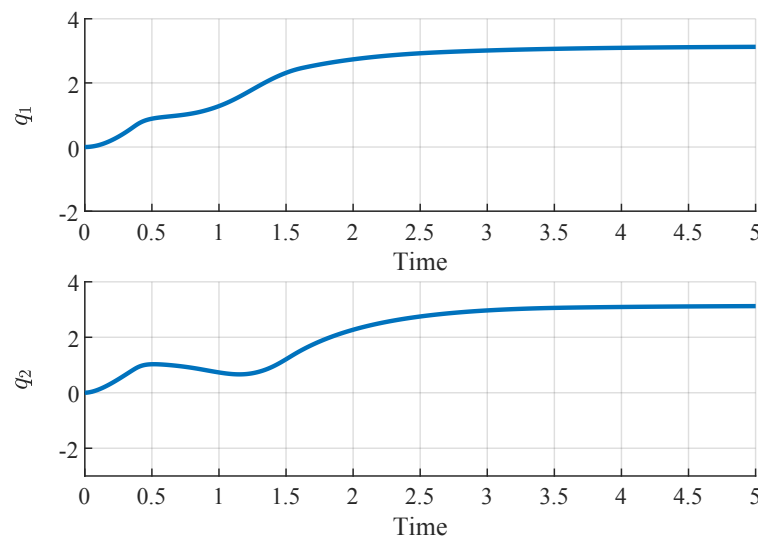


Figure 10. Angular position trajectory of the joints.

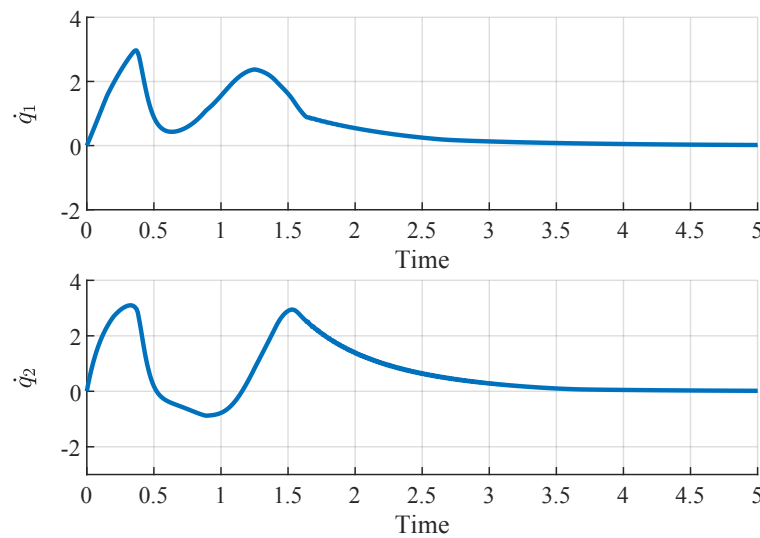


Figure 11. Angular velocity trajectory of the joints.

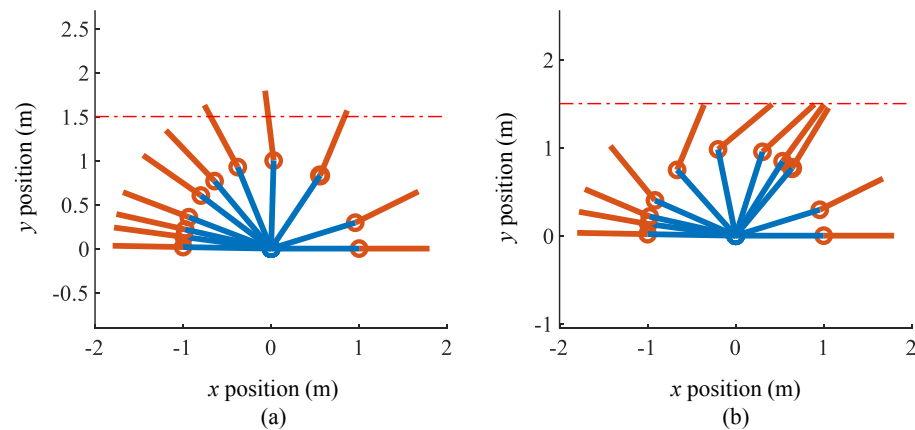


Figure 12. Two-link robot manipulator with physical constraints. (a) NFTSMC only; (b) the CBF-QP was utilized based on the nominal NFTSM controller. The dashed line is state constraint. The blue and orange line are joint-1 and joint-2, respectively.

5. Conclusions

In this paper, a novel terminal sliding surface is introduced to improve the convergence rate of the conventional nonsingular terminal sliding mode control. We illustrate the effect of model uncertainties and external disturbances of the Euler–Lagrange system, and the high control performance and robustness of the proposed controller are guaranteed. Furthermore, the CBF-QP control strategy ensures that the system remains safe with the formulated state constraints. The simulation results illustrate the control performance and effectiveness of the proposed control strategy. This control strategy provides a general and practical approach for any mechanical system formulated as a Euler–Lagrange system.

Author Contributions: Methodology, G.S.; writing—original draft, G.S.; supervision, Q.Z. All authors have read and agreed to the published version of the manuscript.

Funding: This research received no external funding.

Data Availability Statement: Data is contained within the article. The data presented in this study are available in Section 4.

Conflicts of Interest: The authors declare no conflict of interest.

Abbreviations

The following abbreviations are used in this manuscript:

SMC	Sliding mode control
TSMC	Terminal sliding mode control
ATNTSM	Three letter acronym
NFTSMC	Nonsingular fast terminal sliding mode control
QP	Quadratic programming
CBF	Control barrier function

References

- Cai, X.; de Queiroz, M. Adaptive rigidity-based formation control for multirobotic vehicles with dynamics. *IEEE Trans. Control Syst. Technol.* **2015**, *23*, 389–396. [[CrossRef](#)]
- Roy, S.; Roy, S.B.; Kar, I.N. Adaptive-Robust Control of Euler-Lagrange Systems with Linearly Parametrizable Uncertainty Bound. *IEEE Trans. Control Syst. Technol.* **2018**, *26*, 1842–1850. [[CrossRef](#)]
- Shao, X.; Sun, G.; Yao, W.; Liu, J.; Wu, L. Adaptive Sliding Mode Control for Quadrotor UAVs with Input Saturation. *IEEE/ASME Trans. Mechatron.* **2022**, *27*, 1498–1509.
- De Marinis, A.; Iavernaro, F.; Mazzia, F. A minimum-time obstacle-avoidance path planning algorithm for unmanned aerial vehicles. *Numer. Algorithms* **2022**, *89*, 1639–1661.
- Shakouri, A.; Shakouri, A. Prescribed-Time Control for Perturbed Euler-Lagrange Systems with Obstacle Avoidance. *IEEE Trans. Autom. Control* **2022**, *67*, 3754–3761. [[CrossRef](#)]
- Mobayen, S.; Alattas, K.A.; Assawinchaichote, W. Adaptive continuous barrier function terminal sliding mode control technique for disturbed robotic manipulator. *IEEE Trans. Circuits Syst. I Regul. Pap.* **2021**, *68*, 4403–4412.
- Chen, L.; Guo, Y.; Li, C.; Huang, J. Satellite Formationcontainment flying control with collision avoidance. *AIAA J. Aerosp. Inf. Syst.* **2018**, *15*, 253–270.
- Spong, M.W.; Hutchinson, S.; Vidyasagar, M. *Robot Dynamics and Control*; John Wiley & Sons: Hoboken, NJ, USA, 2008.
- Andrade, R.; Raffo, G.V.; Normey-Rico, J.E. Model predictive control of a tilt-rotor UAV for load transportation. In Proceedings of the 2016 European Control Conference (ECC), Aalborg, Denmark, 19 June–1 July 2016; pp. 2165–2170.
- Scaglioni, B.; Previtera, L.; Martin, J.; Norton, J.; Obstein, K.L.; Valdastrì, P. Explicit Model Predictive Control of a Magnetic Flexible Endoscope. *IEEE Robot. Autom. Lett.* **2019**, *4*, 716–723. [[PubMed](#)]
- Song, Z.; Sun, K. Adaptive Sliding Mode Tracking Control for Uncertain Euler-Lagrange System. *IEEE Access* **2019**, *7*, 56817–56825.
- Li, H.; Li, X. Distributed Model Predictive Consensus of Heterogeneous Time-Varying Multi-Agent Systems: With and Without Self-Triggered Mechanism. *IEEE Trans. Circuits Syst. I Regul. Pap.* **2020**, *67*, 5358–5368.
- Mehrabian, A.; Khorasani, K. Distributed Formation Recovery Control of Heterogeneous Multiagent Euler–Lagrange Systems Subject to Network Switching and Diagnostic Imperfections. *IEEE Trans. Control Syst. Technol.* **2016**, *24*, 2158–2166. [[CrossRef](#)]
- Hou, H.; Yu, X.; Xu, L.; Rsetam, K.; Cao, Z. Finite-Time Continuous Terminal Sliding Mode Control of Servo Motor Systems. *IEEE Trans. Ind. Electron.* **2020**, *67*, 5647–5656.
- Feng, Y.; Yu, X.; Man, Z. Non-singular terminal sliding mode control of rigid manipulators. *Automatica* **2002**, *38*, 2159–2167.
- Zhai, J.; Xu, G. A novel non-singular terminal sliding mode trajectory tracking control for robotic manipulators. *IEEE Trans. Circuits Syst. II Express Briefs* **2021**, *68*, 391–395. [[CrossRef](#)]
- Labbadi, M.; Cherkaoui, M. Robust adaptive nonsingular fast terminal sliding-mode tracking control for an uncertain quadrotor UAV subjected to disturbances. *ISA Trans.* **2020**, *99*, 290–304. [[PubMed](#)]
- Moser, D.; Schmied, R.; Waschl, H.; del Re, L. Flexible Spacing Adaptive Cruise Control Using Stochastic Model Predictive Control. *IEEE Trans. Control Syst. Technol.* **2018**, *26*, 114–127.
- Hu, J.; Zhang, H.; Liu, L.; Zhu, X.; Zhao, C.; Pan, Q. Convergent Multiagent Formation Control With Collision Avoidance. *IEEE Trans. Robot.* **2020**, *36*, 1805–1818.
- Lee, J.H. Model predictive control: Review of the three decades of development. *Int. J. Control Autom. Syst.* **2011**, *9*, 415–424.
- Zhang, Z.; Wu, Y. Adaptive Fuzzy Tracking Control of Autonomous Underwater Vehicles with Output Constraints. *IEEE Trans. Fuzzy Syst.* **2021**, *29*, 1311–1319. [[CrossRef](#)]
- Zhang, J.; Li, K.; Li, Y. Output-Feedback Based Simplified Optimized Backstepping Control for Strict-Feedback Systems with Input and State Constraints. *IEEE/CAA J. Autom. Sin.* **2021**, *8*, 1119–1132.
- Jiang, X.; Zhao, D. Event-triggered fault detection for nonlinear discrete-time switched stochastic systems: A convex function method. *Sci. China Inf. Sci.* **2021**, *64*, 200204. [[CrossRef](#)]
- Zhang, T.; Deng, F.; Sun, Y.; Shi, P. Fault estimation and fault-tolerant control for linear discrete time-varying stochastic systems. *Sci. China Inf. Sci.* **2021**, *60*, 200201.
- Ames, A.D.; Grizzle, J.W.; Tabuada, P. Control Barrier Function based Quadratic Programs with Application to Adaptive Cruise Control. In Proceedings of the 53rd IEEE Conference on Decision and Control, Los Angeles, CA, USA, 15–17 December 2014; pp. 6271–6278.

26. Wang, L.; Ames, A.D.; Egerstedt, M. Safety Barrier Certificates for Collisions-Free Multirobot Systems. *IEEE Trans. Robot.* **2017**, *33*, 661–674.
27. Wang, L.; Ames, A.D.; Egerstedt, M. Safe certificate-based maneuvers for teams of quadrotors using differential flatness. In Proceedings of the 2017 IEEE International Conference on Robotics and Automation (ICRA), Singapore, 29 May–3 June 2017; pp. 3293–3298.
28. Grandia, R.; Taylor, A.J.; Ames, A.D.; Hutter, M. Multi-layered safety for legged robots via control barrier functions and model predictive control. In Proceedings of the 2021 IEEE International Conference on Robotics and Automation (ICRA), Xi'an, China, 30 May–5 June 2021; pp. 8352–8358.
29. Hsu, S.C.; Xu, X.; Ames, A.D. Control barrier function based quadratic programs with application to bipedal robotic walking. In Proceedings of the 2015 American Control Conference (ACC), Chicago, IL, USA, 1–3 July 2015; pp. 4542–4548.
30. Yu, S.; Yu, X.; Shirinzadeh, B.; Man, Z. Continuous finite-time control for robotic manipulators with terminal sliding mode. *Automatica* **2005**, *41*, 1957–1964. [[CrossRef](#)]
31. Ames, A.D.; Coogan, S.; Egerstedt, M.; Notomista, G.; Sreenath, K.; Tabuada, P. Control barrier functions: Theory and applications. In Proceedings of the 2019 18th European Control Conference (ECC), Napoli, Italy, 25–28 June 2019; pp. 3420–3431.
32. Ames, A.D.; Xu, X.; Grizzle, J.W.; Tabuada, P. Control Barrier Function Based Quadratic Programs for Safety Critical Systems. *IEEE Trans. Autom. Control* **2017**, *62*, 3861–3876.
33. Nguyen, Q.; Sreenath, K. Exponential control barrier functions for enforcing high relative-degree safety-critical constraints. In Proceedings of the 2016 American Control Conference (ACC), Boston, MA, USA, 6–8 July 2016; pp. 322–328.
34. Xu, X. Constrained control of input-output linearizable systems using control sharing barrier functions. *Automatica* **2018**, *87*, 195–201.

Disclaimer/Publisher's Note: The statements, opinions and data contained in all publications are solely those of the individual author(s) and contributor(s) and not of MDPI and/or the editor(s). MDPI and/or the editor(s) disclaim responsibility for any injury to people or property resulting from any ideas, methods, instructions or products referred to in the content.